EFFECTS OF PROTON-INDUCED DISPLACEMENT DAMAGE ON GALLIUM NITRIDE POWER AMPLIFIER RF PERFORMANCE

By

NATHAN ELMER IVES

Thesis

Submitted to the Faculty of the

Graduate School of Vanderbilt University

in partial fulfillment of the requirements

for the degree of

MASTER OF SCIENCE

in

Electrical Engineering

August, 2015

Nashville, Tennessee

Approved:

Professor Ronald D. Schrimpf

Professor Arthur F. Witulski

ACKNOWLEDGEMENTS

I would like to acknowledge and express my sincere gratitude to all of my professors and colleagues at Vanderbilt University in the Radiation Effects and Reliability group. First and foremost I thank my advisor, Dr. Ron Schrimpf, for his guidance and direction in this work. Many others provided essential contributions to this work, including Professors Art Witulski, Dan Fleetwood, Lloyd Massengill, Timothy Holman, Ralph Bruce, and the folks at ISDE. Thanks to Enxia Zhang, Mike McCurdy, and Jin Chen for assistance in running my experiments and thanks to Andrew Sternberg for assistance with soldering.

I also feel the need to express my deep gratitude for my undergraduate advisor, Dr. Aaron Hawkins, and all of the BYU professors in the IMMERSE undergraduate research program. They gave me my first opportunity to conduct academic research in a cleanroom fabrication facility and encouraged me to attend graduate school.

My deepest feelings of gratitude are for my family and friends for their support. I thank my parents Eldon and Sharon Ives for nurturing my curious mind, for their never-ending encouragement, and for making sacrifices on my behalf. Most of all I must acknowledge and express gratitude to my wonderful wife, Katy Ives, for supporting me in every way possible through my education, and to my wonderful children Evelyn and Ephraim, who enhance my life and give meaning to my work.

I would also like to thank the Defense Threat Reduction Agency, who provided financial support and direction for this work.

TABLE OF CONTENTS

LIST OF TABLES

LIST OF FIGURES

CHAPTER I

Introduction

High frequency RF and microwave communications systems for military, space, and telecommunications applications require efficient power amplifiers with high power density. In the quest for faster and more reliable RF communication systems, many advances have been made in the development of high frequency power transistors. One of the modern materials used to fabricate power transistors is gallium nitride (GaN), which is used to make high electron mobility transistors (HEMTs). Gallium nitride has many desirable material properties that make it well suited for devices operated at high frequency, high power, and in extreme temperatures [1]. GaN HEMTs have a high concentration of carriers, high carrier velocity, and higher power density than competing technologies [2]. A background on III-V compound semiconductor materials, including GaN, and the history of III-V HEMTs will be presented in Chapter II.

The superior material properties of GaN make GaN-based devices ideal candidates for telecommunications and spacecraft systems. The harsh environment of space not only includes extreme temperatures, but also high levels of radiation compared to the terrestrial environment. The effects of radiation on electronic devices intended for operation in space environments must be well understood in order to avoid unwanted degradation of device parameters and potential catastrophic failures. The effects of ionizing and non-ionizing damage due to radiation on GaN HEMTs will be discussed in detail in Chapter III.

The purpose of this work is to investigate the radiation hardness of GaN HEMTs, to understand the relationship between device-level degradation and circuit-level RF parameter degradation, to identify potential failure mechanisms, and suggest mitigation techniques. The experimental methodology of this work is presented in Chapter IV.

The approach of this work is to consider the perspective of the RF designer and potential customers of GaN HEMTs in telecommunications, space, or military applications. Using commercial-off-the-shelf (COTS) parts, results were obtained by irradiating GaN HEMTs to 10 keV X-rays and 1.8 MeV protons while measuring DC current-voltage characteristics, S-parameters, and RF power output. Experimental data was taken from devices fabricated by two different manufacturers (RFMD and Cree). Using the 2-port S-parameters, we analyze the Rollett stability factor of the GaN amplifiers as a function of radiation damage, and make conclusions on the effects of displacement damage on amplifier stability. A comparison between the DC and RF performance of the two sets of devices and discussion of the degradation mechanisms is given in Chapter V. Conclusions on the effects of displacement damage on RF parameters in GaN HEMTs, along with suggestions for mitigation techniques will be provided in Chapter VI.

CHAPTER II

Background

The invention of the transistor is arguably the most important of the 20th century. The use of semiconductors in our electronic circuits has been groundbreaking, and paved the way for the rapid development of smaller and faster computers and electronics that continue to shape our way of life. Elemental semiconductor crystals such as germanium and silicon have been pivotal in the development of semiconductor technology, but the intrinsic material properties of each have their limitations, such as the indirect bandgap of silicon. Compound semiconductors such as gallium arsenide (GaAs) and gallium nitride (GaN) have long been considered and studied for their desirable material properties such as high carrier mobility or direct bandgap.

Elemental semiconductor materials such as silicon and germanium are part of group IV or the carbon group, which have four valence electrons. Combinations of group III and group V elements (three and five valence electrons), or group II and group VI elements (two and six valence electrons) produce binary compound semiconductor materials such as GaN or ZnS. Ternary compounds such as AlGaN and quaternary compounds such as InGaZnO have also been fabricated and have important material properties. The focus of this chapter is on the family of III-V binary compound semiconductors, and in particular III-Nitrides such as GaN.

Table I. Elements commonly used in compound semiconductors.

II	III	IV	V	VI
	B 5	C 6	N 7	O 8
	Al 13	Si 14	P 15	S 16
Zn 30	Ga 31	Ge 32	As 33	Se 34
Cd 48	In 49	Sn 50	Sb 51	Te 52

III-V binary compound semiconductors are very important for special electronics applications such as optoelectronics and high frequency switching. Classic examples of III-V materials are gallium arsenide (GaAs), gallium nitride (GaN), and indium arsenide (InAs). Many III-V compound semiconductors have a direct bandgap, allowing them to absorb or emit light when electrons are excited to the conduction band or relax to the valence band. III-V compounds can be used to fabricate light emitting diodes (LEDs) of different wavelengths depending on the bandgap of the material. For example, blue through ultraviolet wavelength light can be produced using GaN, either alone or in combination with ternary compounds.

Gallium nitride (GaN) has many outstanding properties which set it apart from other elemental or compound semiconductors for high frequency switching applications. GaN devices offer high carrier velocity, high breakdown voltage, high power density, and superior thermal properties [1]. In addition, GaN devices exhibit channel carrier densities five times higher than GaAs devices [3]. A table of material properties provides some comparison of various semiconductor materials in Table II, where E_g is the bandgap, μ is

the electron mobility at 300 K, v_{sat} is the saturation velocity, K_s is the relative permittivity, f_T is the cutoff frequency, and T_{max} is the maximum allowable temperature for operation.

Table II: Properties of various semiconductor materials.

Material	E_g (eV)	μ (cm^2/V-s)	v_{sat} (10^7 cm/s)	K_s	f_T (GHz)	T_{max} (°C)
Si	1.12	1300	1	11.9	>40	300
GaAs	1.42	8,500	0.8	12.8	>150	300
InP	1.35	10,000	2.2	12.5	>300	425
4H-SiC	3.26	700	2	10	>20	600
GaN	3.4	2,000	2.5	9.5	>180	700

The crystal structure of GaN is fundamentally different from that of silicon, and is responsible for many of the material properties and effects that make GaN attractive. Elemental silicon and germanium form a diamond lattice structure, whereas GaN and many other III-V compounds form a Wurtzite lattice structure as shown in Fig. 2.1. The asymmetry of the Wurtzite lattice gives rise to spontaneous polarization, which enables the formation of the electron channel in GaN high electron mobility transistors (HEMTs). The unit cell of the silicon diamond lattice has a single lattice constant, a = 5.43 Å. The unit cell of the GaN Wurtzite structure has two lattice constants, a = 3.19 Å, and c = 5.18 Å. The smaller lattice constants of GaN mean that the atoms are more tightly bound and require more energy to displace from the lattice.

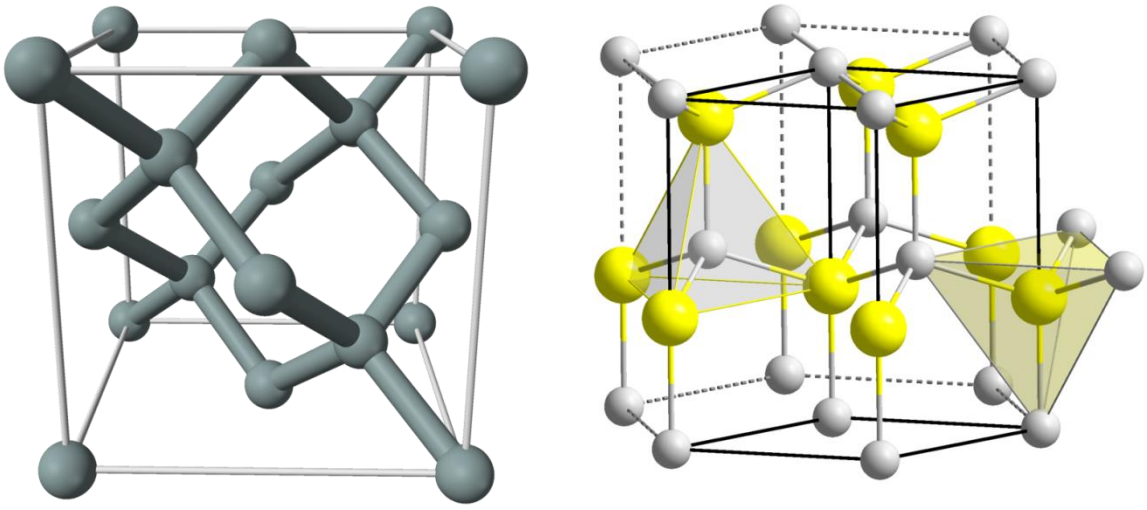

(a) Diamond Lattice (b) Wurtzite Lattice

Fig. 2.1. (a) Diamond lattice structure. (b) Wurtzite lattice structure.

GaN is typically used to fabricate high electron mobility transistors or HEMTs, rather than conventional MOSFETs or MESFETs. The high electron mobility transistor is also known by many other names. Some of these names include modulation-doped field-effect transistor (MODFET), two-dimensional electron gas field-effect transistor (TEGFET), and heterojunction field-effect transistor (HFET) [4], [5]. This work refers to it simply as a HEMT.

The HEMT is one solution for devices requiring high carrier density and high carrier mobility for high frequency operation. As conventional field effect transistors scale, higher carrier concentrations are required. But as the number of dopant atoms increases, the carrier mobility decreases. This decrease in carrier mobility occurs because the dopant atoms cause ionized impurity scattering. A good example of this is silicon,

where the mobility of lightly doped Si may be ~1300 cm^2/V-s, but once doped to 10^{18} cm^{-3}, the mobility decreases to ~200 cm^2/V-s [4].

The HEMT solves this problem of scattering by utilizing a technique called modulation doping. Modulation doping is achieved by forming a heterojunction between a highly doped wide bandgap material (such as n-$Al_xGa_{1-x}N$) and an undoped narrow bandgap material (such as GaN). The electrons in the highly doped material diffuse into the undoped material, and are trapped in a quantum well formed by the band structure. The severe band bending is caused by an electric displacement field due to the strain-induced piezoelectric polarization between the $Al_xGa_{1-x}N$ and GaN layers. This thin layer where electrons are contained is referred to as the two-dimensional electron gas or 2DEG. The 2DEG produces a high concentration of carriers without the unwanted side effects of ionized impurity scattering. This in turn allows a HEMT to discharge capacitances faster, allowing for higher frequency operation. Fig. 2.2 shows the cross section of a generic GaAs HEMT, with ohmic contacts and a Schottky gate contact. Fig. 2.3 shows the band diagram featuring a quantum well in which the electrons reside.

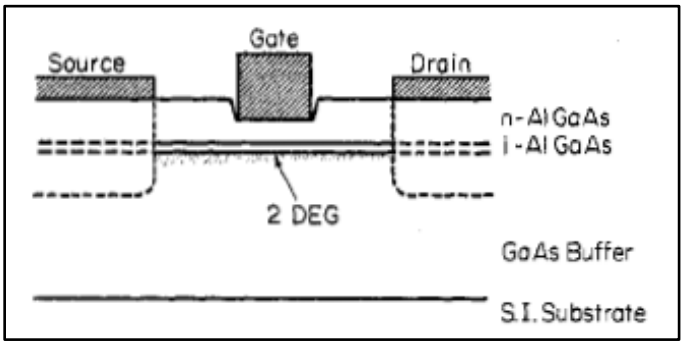

Fig. 2.2. Cross sectional view of a gallium arsenide high electron mobility transistor [5].

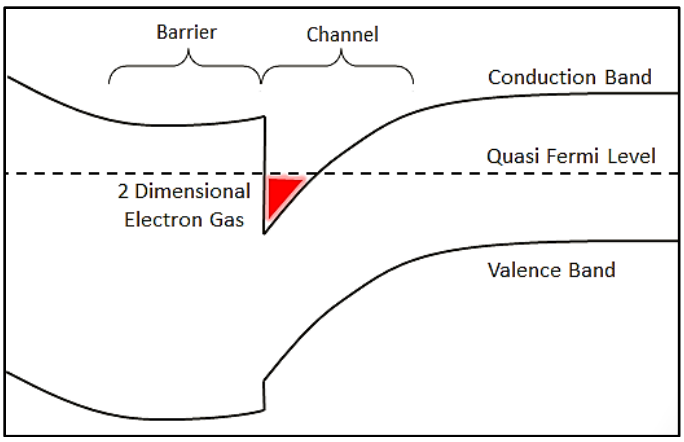

Fig. 2.3. Band diagram of a generic HEMT, featuring a quantum well and 2DEG.

The concept of constructing GaAs-AlGaAs superlattices to achieve high mobilities was proposed by Esaki and Tsu at IBM in 1970 [6], and eventually led to the idea of modulation doping. Modulation-doping in GaAs-AlGaAs to achieve high carrier mobility at room temperature was first demonstrated by Dingle et al. at Bell Labs in 1978 [7]. A working modulation-doped field-effect transistor (MODFET or HEMT) was later demonstrated in 1980 [5]. Since then, HEMTs have been fabricated from a variety of compound semiconductors. In 1993, the first HEMT was fabricated from GaN-AlGaN by Khan et al. [8]. Fabrication challenges and reliability issues for GaN HEMTs have prevented them from becoming commercially viable option for power applications until recently, and continue to be a concern [1], [3], [9]. Overall, it has taken several decades for the ideas and concepts of modulation doping of compound semiconductors to develop into the modern GaN HEMTs that are commercially available today.

CHAPTER III

Effects of Radiation on GaN HEMTs

As gallium nitride HEMTs are considered for use in telecommunications, space, and military applications, the effects of radiation on the lifetime and performance of GaN HEMTs must be well understood. Previous studies show that GaN is more robust to radiation damage than other semiconductor materials [10], due partly to the high lattice displacement threshold energy (E_d) of III-Nitride materials, compared to other III-V compounds and silicon. However, damage from terrestrial and space radiation can and does affect the performance of GaN HEMTs. Damage to electronics may be caused by naturally occurring neutrons, protons, heavy ions, electrons, muons, and photons such as X-rays and γ-rays.

Radiation outside the Earth's atmosphere contains a wide spectrum of ions ranging from protons to heavy ions. The amount and type of radiation varies greatly with altitude, location, and time [11]. Trapped protons and electrons dominate the flux spectrum in the near-Earth space environment. This is due to the Earth's magnetic field, which traps protons and electrons in the Van Allen radiation belts. Background galactic cosmic rays (GCRs) and solar wind dominate the space environment further away from Earth. Solar disturbances such as coronal mass ejection may occur at any time and wreak havoc on space electronics. Solar activity tends to follow an 11-year cycle with peaks at solar maximum and lows at solar minimum. A plot of the flux environment in low-Earth orbit (LEO) was generated using the CREME96 SEE rate prediction tool in Fig. 3.1.

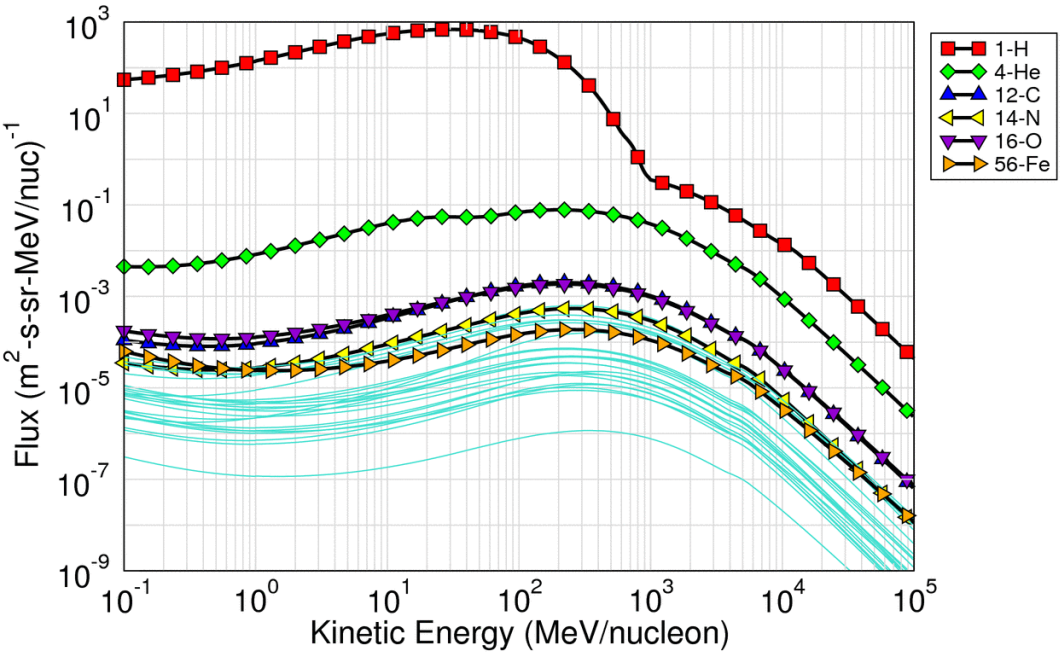

Fig. 3.1. CREME96 simulation of the flux environment at 780 km altitude and with 100 mils of aluminum shielding at solar minimum.

In addition to the protons and heavy ions in the space environment, neutrons occur naturally in the terrestrial environment, and nuclear reactors emit both neutrons and γ-rays. Neutrons cause non-ionizing damage to semiconductor materials, and may cause nuclear collisions which create secondary ionizing particles. The effects of radiation on electronics due to ionizing and non-ionizing radiation can generally be classified into four main areas: total ionizing dose (TID) effects, dose rate effects, displacement damage effects, and single event effects (SEE).

Total Ionizing Dose

Total ionizing dose (TID) is a measure of the amount of ionizing damage from high energy X-rays, γ-rays, or charged particles such as protons and heavy ions. This

damage typically manifests itself as trapped charge in an oxide layer, surface, or interface. Charged particles, X-rays and γ-rays deposit energy and create electron-hole pairs. The average energy required to generate an electron-hole pair in SiO_2 is ~18 eV. The electrons often get swept away due to electric fields present in the device, leaving a net positive charge in the oxide or interface. TID has traditionally been a problem for devices with thick oxide layers, and may cause shifts in threshold voltage and increase leakage current.

The effects of TID on GaN HEMTs have been studied previously, and the general consensus is that GaN-based devices are very tolerant to ionizing radiation [12], [13]. One reason for this is because conventional GaN HEMTs do not have gate oxides, and instead they use Schottky gate contacts [14]. However, defects in the AlGaN-GaN interface, as well as the introduction of gate oxide layers (i.e., MOS-HEMTs) can increase susceptibility to TID [15].

Displacement Damage

A bigger concern than TID for GaN HEMTs is the amount of displacement damage in the crystal lattice structure. If an incident energetic particle such as a neutron or proton collides with the nucleus of a lattice atom, the primary knock-on atom (PKA) may be displaced from the lattice if the incident particle has sufficient energy ($E > E_d$), where E_d is the lattice displacement energy. The lattice displacement energy is inversely proportional to the lattice constant [16]. A table of lattice displacement threshold energy E_d and the lattice constants of semiconductor materials is given in Table III. If a lattice atom is displaced, it may result in a stable defect or trap, which will affect the

performance of the HEMT by removing carriers from the 2DEG and decreasing the mobility [16]. The defects may also result in threshold voltage shift, decrease in transconductance, and decrease in drain saturation current [10], [16]–[18].

Table III. Semiconductor materials, displacement threshold energies [19], and lattice constants.

Material	**E_d (eV)**	**Lattice Constant (Å)**
InAs	7.4	a = 6.06
GaAs	9.5	a = 5.65
Si	12.9	a = 5.43
GaN	19.5	a = 3.19 c = 5.18
4H-SiC	21.3	a = 3.07 b = 10.05

Neutrons are not charged particles, so as neutrons pass through a crystal, energy is lost primarily to nuclear stopping, not electronic stopping. Most of the nuclear collisions result in lattice displacement, with only a small percentage of collisions resulting in secondary particles that cause ionizing effects [20]. Therefore, neutron irradiation is a simple and straightforward method of determining the effects of displacement damage in a semiconductor crystal. On the other hand, charged particles such as protons and heavy ions pass through a crystal lattice structure and cause both ionizing damage and non-ionizing damage, making it difficult to accurately quantify displacement damage.

Nuclear reactors such as the one at OSU-NRL are used for neutron testing, since they emit both gamma rays and neutrons. In order to test a part for neutron radiation, the

device must be placed near a nuclear reactor with a high n/γ ratio, typically with some shielding from the γ-rays. This creates some problems, such as difficulty in making prompt measurements in close proximity to the reactor, and the fact that device may be radioactively "hot" post-irradiation. Devices are then typically shipped back to a lab where electrical characterization is made.

According to the ASTM designation F1190, annealing starts to occur within seconds to days. The annealing slows over time, but may continue for up to 2 months. The ASTM recommends that electrical measurements be taken within 2 days of irradiation. Since annealing of defects begins immediately after irradiation, waiting several days before performing electrical measurements is not optimal.

One alternative is to use protons rather than neutrons, and to calculate the ratio of ionizing damage to non-ionizing damage. The amount of non-ionizing energy loss is known as NIEL, and NIEL can frequently be correlated linearly with device degradation. NIEL can be calculated using tools such as SRIM for proton with various LETs. Table IV shows SRIM calculations of NIEL for protons with various LETs used in a study by Hu et al. in 2004 [17]. The table includes the maximum proton fluence used at each LET in the study and the equivalent TID.

Table IV: SRIM calculations of non-ionizing energy loss (NIEL) for proton irradiation in GaN [17].

Energy Loss	1.8 MeV	15 MeV	40 MeV	105 MeV
IEL (keV/Ion)	114	26.2	12.2	6.1
NIEL (eV/Ion)	3.1	0.27	0.1	0.05
Maximum Fluence (cm^{-2})	10^{12}	5×10^{10}	10^{11}	10^{13}
Total Ionizing Dose (rads)	1.1×10^{6}	1.7×10^{4}	1.6×10^{4}	8.0×10^{5}

Some of the effects of displacement damage on GaN HEMTs have been studied previously [10], [16]–[18], [21], [22]. Lower energy protons at high fluence levels have a larger effect than higher energy protons at lower fluence levels [23] because of the higher NIEL of low energy protons as seen in Table IV.

In addition to the effects of displacement damage on DC parameters such as I_D, g_m, and V_T, a few studies report effects on RF performance. Kalavagunta et al. report an increase in DC-RF dispersion or gate lag with 1.8 MeV protons at high fluence levels (10^{13} cm^{-2}) [21]. Chen et al. report a decrease in forward gain S_{21}, and a decrease in cutoff frequency f_T [22]. Of particular note, Chen attributes some of the RF degradation to changes in device impedance, citing impedance mismatch as a possible cause.

The question of whether changes in device impedance could cause mismatch and affect the stability of a GaN-based power amplifier is one of the driving questions behind this work. This work investigates the effects of displacement damage on small signal S-parameters, amplifier stability, and output power. The effects of V_T shift on the gain will

be addressed along with possible impacts on the mode of operation of the amplifier circuit.

Single Event Effects

The effects of single event particle strikes in GaN HEMTs have not been thoroughly investigated. Only a handful of publications exist in this area of research [24]. Single event effects (SEEs) include a wide range of effects including both soft errors and hard errors. A soft error occurs when a heavy ion strikes a semiconductor substrate, creating electron-hole pairs, and charge collects at nodes in the circuit, resulting in transient signals. Sometimes catastrophic failures (hard errors) occur when a heavy ion strikes a sensitive region in the device and permanently cause increased leakage current or render the device inoperable. Single event burnout (SEB) occurs when a particle strikes an FET in the off state and the resulting ion track activates a parasitic bipolar transistor causing a feedback mechanism which leads to secondary breakdown [25]. A single event gate rupture (SEGR) occurs when a particle strikes under the gate, creating electron hole pairs, and the holes accumulate under the gate, creating a strong electric field and causing dielectric breakdown to occur.

In 2007, Bazzoli et al. were the first to study SEEs in GaN HEMTs [26]. They reported soft errors using heavy ions with LET of 39 MeV-cm^2/mg which temporarily increase gate leakage current. They also reported catastrophic failures using heavy ions with V_D = 53 V, V_G = -20 V, and particle LET of 60 MeV-cm^2/mg. These phenomena appear to be similar to single event gate rupture (SEGR), despite a lack of gate oxide. No single event burnout (SEB) could be induced.

In 2011, Kuboyama et al. reported several different types of permanent damage using heavy ions, including enhanced charge collection with Ne ions and increased leakage current with Ar and Kr ions [27]. In 2013, Rostewitz et al. reported two different failure modes: increased drain and gate leakage at 125 V drain voltage, and SEB using drain voltage of 155 V and particle LET of 48 MeV-cm^2/mg [28].

The robust nature of GaN HEMTs to total ionizing dose damage and minimal degradation due to displacement damage leads to the conclusion that single event effects in GaN HEMTs merit further study [14]. The work of this thesis, however, focuses on displacement damage as a potential hazard to the overall lifetime and performance of GaN HEMTs in the space environment. Single event effects are outside the scope of this work.

CHAPTER IV

Experimental Methodology

Device Description and Preparation

For this work, commercially available devices were tested from the manufacturers RFMD (now Qorvo) and Cree. RFMD model RF3826 is a 9-Watt, GaN-on-SiC HEMT. Cree model CGH40006P is an 8-Watt, GaN-on-SiC HEMT. Both models are depletion mode AlGaN-GaN HEMTs, requiring a negative gate voltage to turn off. Both GaN HEMTs include gate-connected field plates and source-connected field plates. Both HEMTs are intended for linear operation over a broad frequency spectrum. Specifications for the two GaN HEMTs are included in Table V, where P_{out} is the output power, BW is the bandwidth, V_{DD} *Typ*. is the typical drain voltage, PAE is power-added efficiency, η_{drain} is the drain efficiency, and L is the channel length. The only major design difference between the two GaN HEMT is the addition of a passive input matching network included on the RFMD package, which is wire bonded to the HEMT die. The Cree device is an unmatched HEMT. Three devices from each manufacturer were tested for radiation effects, for a total of six devices tested.

Table V: GaN HEMT device specifications.

Model	P_{out} (W)	Gain (dB)	BW (GHz)	V_{DD} *Typ*. (V)	PAE (%)	η_{drain} (%)	L (µm)
RF3826	9	12	0 - 2.5	28	45	--	0.5
CGH40006P	8	11 - 13	1 - 6	28	--	53 - 65	0.4

Commercially available evaluation boards were used as test fixtures for the GaN HEMTs; models RF3626PCBA-410 and CHG40006P-TB for the respective RFMD and Cree devices. These test boards enable DC bias and 50-Ω impedance matched RF input/output connections allowing convenient and reliable electrical measurements of both DC and RF parameters of the device without additional equipment such as bias tees. Both evaluation boards have large aluminum heat sinks attached to the PCB to prevent excessive heating of the GaN HEMT.

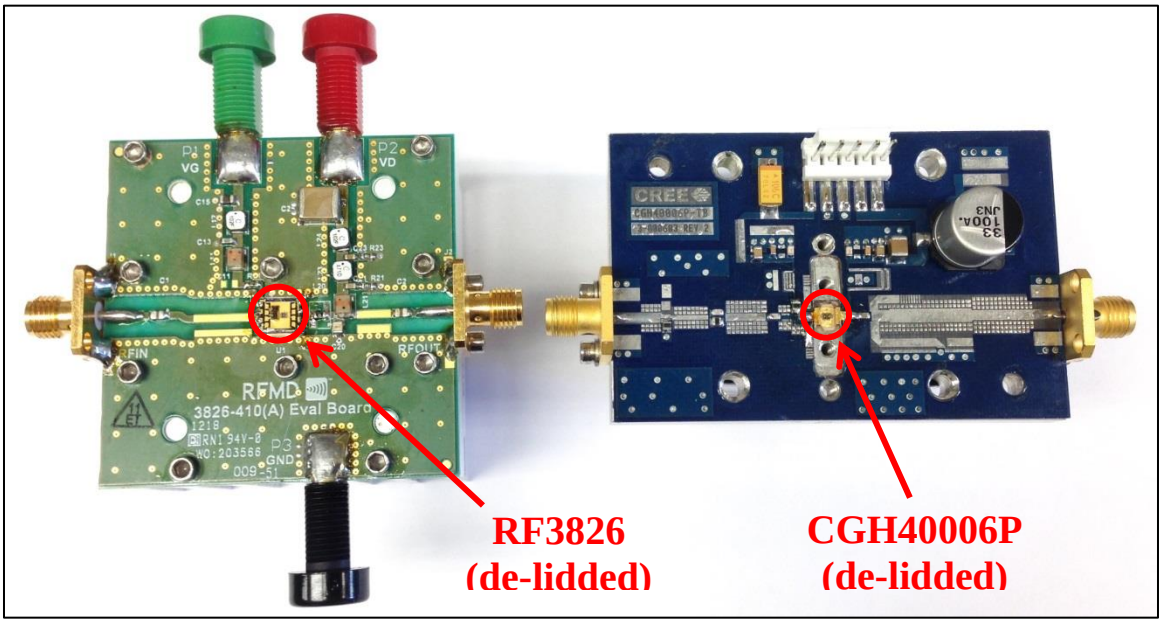

Fig. 4.1. Evaluation boards used in experiments.

The ceramic lids on the device packages were removed prior to irradiation. A heat gun or hotplate was used to soften the adhesive, and tweezers were used to remove the lids. Both device packages have a large metal ground pad on the bottom side of the package with the source tied to ground to dissipate thermal energy directly into the heat sink. The gate and drain connections for both devices are on the edges of the packages.

The RF3826 devices were wave soldered to the PCB. The CGH40006P devices were attached to the aluminum heat sink using silver epoxy and the gate/drain leads were connected with solder.

S-Parameters

The scattering parameters or S-parameters of a two-port electrical network are the elements (S_{ij}) of the scattering matrix [**S**] which describes the transmitted and reflected signals at each side of the two-port network. Unlike Z-parameters or Y-parameters which use current or voltage inputs, and have short-circuit or open-circuit terminations, S-parameters measure transmitted and reflected power with 50-Ω matched terminations. This allows high frequency measurements for RF and microwave circuits.

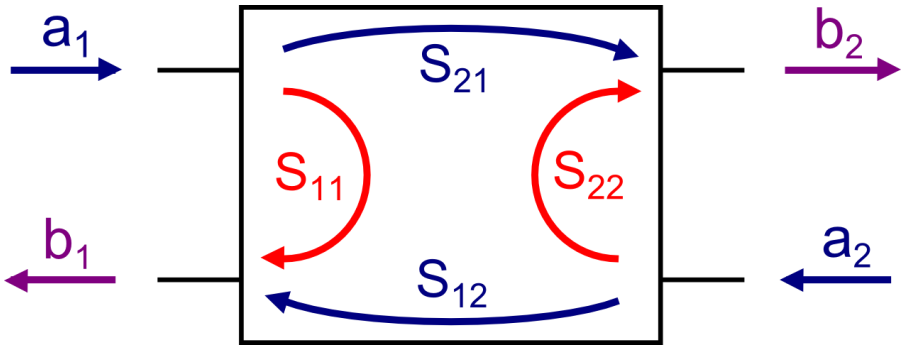

Fig. 4.2. Block diagram of S-parameter measurement.

The signals a_1 and a_2 are incident waves (small signal RF power signals) at a given frequency, and the signals b_1 and b_2 are either transmitted or reflected waves. The S-parameters are defined with the following equations:

$$[S] = \begin{bmatrix} S_{11} & S_{12} \\ S_{21} & S_{22} \end{bmatrix}$$

$$\begin{bmatrix} a_1 \\ a_2 \end{bmatrix} = \begin{bmatrix} S_{11} & S_{12} \\ S_{21} & S_{22} \end{bmatrix} \begin{bmatrix} b_1 \\ b_2 \end{bmatrix}$$

S-parameters can be used to describe a passive network or active devices, or some combination of passive and active components. Everything including the cables, connections, microstrip wires, circuit elements, PCB connections, wire bonds, and even solder add parasitic inductance and capacitance contribute to the overall RF response of the electrical network at different frequencies. The S-parameters of a single active device or transistor can be isolated by a process of de-embedding the passive and parasitic elements. The work presented in this thesis takes into consideration the S-parameters of the entire amplifier circuit, including the GaN HEMT and the evaluation board, with all the passive components on the board. This allows an understanding of how the DC degradation of the device affects the circuit as a whole.

Rollett Stability Factor

An amplifier is said to be unconditionally stable if unwanted oscillatory behavior does not occur, regardless of the internal impedance matching of the amplifier. The amplifier is said to be conditionally stable if oscillations may occur if the input or output impedance of the amplifier are not perfectly matched to 50-Ω.

The Smith chart is a useful tool in describing the S-parameters, input reflection coefficients (Γ_{IN}), and output reflection coefficients (Γ_{OUT}) over various frequencies. The input and output reflection coefficients can be mapped onto the same plane as the source and load reflection coefficients, Γ_S and Γ_L producing stability circles which show regions of instability [29].

Fig. 4.3 shows the stability circles for the unconditionally stable case. The input stability circle corresponds to $\Gamma_S = 1$, and the output stability circle corresponds to $\Gamma_L = 1$. The outside of each circle represents the worst possible load or source matching ($\Gamma_L = 1$ or $\Gamma_S = 1$). If the circles intersect or overlap, it means there is a possible region of instability. If the reflection coefficient strays into the region of instability on the Smith chart, oscillations will likely occur. The parameters C_L, r_L, C_S, and r_S are defined as follows:

$$\Delta = S_{11}S_{22} - S_{12}S_{21}$$

$$r_L = \left|\frac{S_{12}S_{21}}{|S_{22}|^2 - |\Delta|^2}\right|$$

$$C_L = \frac{(S_{22} - \Delta S_{11}^*)^*}{|S_{22}|^2 - |\Delta|^2}$$

$$r_S = \left|\frac{S_{12}S_{21}}{|S_{11}|^2 - |\Delta|^2}\right|$$

$$C_S = \frac{(S_{11} - \Delta S_{22}^*)^*}{|S_{11}|^2 - |\Delta|^2}$$

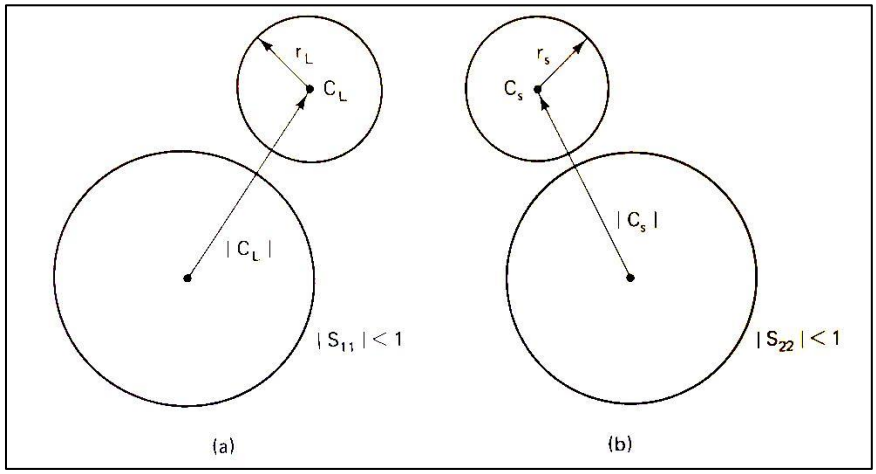

Fig. 4.3. Stability circles for the unconditionally stable case [29]. If the circles intersect or overlap, this indicates a possible region of instability.

In the 1962 paper "The Stability and Power-Gain Invariants of Linear Twoports" J. M. Rollett defined a single factor, K which describes the condition of stability of a two-port electrical network [30]. In reality, there are two conditions (K > 1 and |Δ| < 1) that must be satisfied to guarantee unconditional stability [31], [32]. The K factor and its auxiliary condition Δ allow us to determine the margin of stability without stability circle analysis. The Rollett stability factors *K* and Δ can be derived from the 2-port S-parameters using the following equations:

$$K = \frac{1 - |S_{11}|^2 - |S_{22}|^2 + |\Delta|^2}{2|S_{21}S_{12}|} > 1$$

$$|\Delta| = |S_{11}S_{22} - S_{12}S_{21}| < 1$$

Bias Conditions During Irradiation

The question arises whether to perform the proton irradiation under typical operation conditions, with quiescent drain current and/or RF input signals, or with all pins grounded. All devices in this work were irradiated with drain, gate, and source grounded. Zero applied bias was chosen in order to eliminate extra variables in the testing procedures. Quiescent drain or gate current present during the testing period would contribute heat and cause annealing of defects. It is desirable to avoid perturbing the thermal equilibrium of the device during testing as much as possible. Between irradiation steps, the electrical characteristics were measured quickly in order to avoid device heating. This helps to isolate the effects of radiation from the effects of temperature, self-heating, and prolonged stress on the behavior of the device. It is common to see significant changes in behavior due to prolonged operation of these types of devices [9], making it difficult to isolate changes due to radiation alone.

Another question may arise concerning the influence of electric fields on radiation damage. Testing proton damage under the presence of electric fields does influence the amount of total ionizing dose (TID) damage in semiconductor devices, but does not influence the amount of displacement damage. Since these devices are typically robust to TID, electric fields are not a concern during proton irradiation, and not a necessary part of our testing procedures. We will address TID separately using X-ray testing.

The final question that is frequently asked is whether the results of zero bias irradiation reflect the real-world effects of radiation under typical operating conditions. This type of testing definitely has relevance in real-world scenarios. RF communication circuitry may not always be at operational voltages. In spacecraft missions, it is common to power off electronics in order to conserve power when an orbiting spacecraft passes through the Earth's umbra, or when a spacecraft must travel some distance before the mission begins. Frequently, more damage occurs and accumulates when a device is powered off than during operation, and may cause failures to occur.

TID Testing

In order to conclusively show that device degradation is due to proton-induced displacement damage, not proton-induced TID, the effects of TID must be isolated using X-rays. An ARACOR 10 keV X-ray irradiator was used to irradiate the devices to 1 Mrad (SiO_2). DC current-voltage (I-V) characteristics were taken using the Agilent B1505A Power Device Curve Tracer. S-parameters were measured using the Agilent N5245A PNA-X Microwave Network Analyzer. The drain, gate, and source were grounded during irradiation, and measurements were made post-irradiation.

Proton Testing

The proton energy of 1.8 MeV was chosen for displacement damage testing because it allows convenient comparison to previously published results [10], [16]–[18], [21], [22], and because the amount of NIEL is high compared to higher energy protons. In this work, protons with energy of 1.8 MeV were used up to a fluence of 10^{14} protons/cm^2.

The de-lidded device packages in their evaluation boards were placed inside the Pelletron chamber, with DC and RF cables attached through ports in the sidewall of the chamber. The temperature was ambient room temperature. The drain, gate, and source were grounded during irradiation. Irradiation was paused at logarithmic fluence steps to allow electrical measurements to be taken, beginning at 10^{11} protons/cm^2 and ending at 10^{14} protons/cm^2. The test setup is shown in Fig. 4.4.

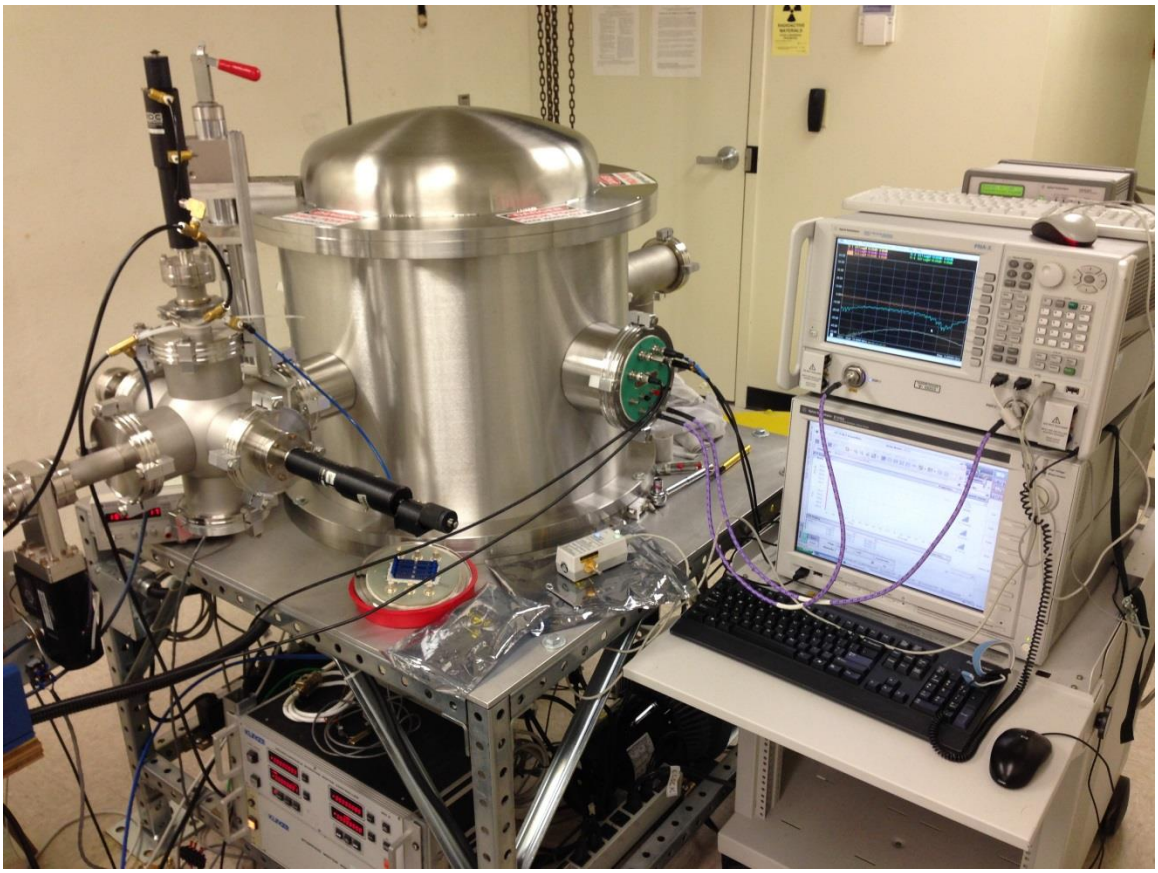

Fig. 4.4. Proton test setup, showing the Pelletron chamber, cables, and the DC and RF measurement equipment.

DC current-voltage (I-V) characteristics were obtained using the Agilent B1505A Power Device Curve Tracer, which was also used to provide DC drain and gate bias during S-parameter and RF power measurements. S-parameters were measured using the Agilent N5245A PNA-X Microwave Network Analyzer. RF input and output power was measured using the HP 435B Power Meter, along with the Agilent E8257D PSG Analog Signal Generator, which was used as the RF source over multiple input power levels. All RF input and output measurements were taken at 1 GHz for model RF3826, and 2 GHz for model CGH40006P.

CHAPTER V

Experimental Results & Discussion

TID Test Results

GaN HEMTs are usually quite tolerant to ionizing radiation [12], [13]. But since we are using protons to test for displacement damage, and protons cause both ionizing and non-ionizing damage, it is important to determine if TID causes significant degradation. In order to ensure that TID does not contribute to threshold voltage shift or other parametric device degradation, we irradiated one of each device with 10 keV X-rays to a dose of 1 Mrad (SiO_2).

While the RFDM GaN HEMTs showed no differences in DC characteristics, S-parameters, or Rollett stability factors after exposure to X-rays, the Cree GaN HEMTs showed a significant change due to X-ray irradiation. The threshold voltage shifted by -0.05 V after exposure to 1 Mrad (SiO_2) as seen in Fig. 5.1.

This was an unexpected result, since the CGH40006P is advertised as a conventional depletion mode GaN-on-SiC HEMT, and there is no indication of any gate oxide layers in the manufacturer datasheet. Despite the threshold voltage shift, there was no decrease in transconductance (g_m), or forward gain (S_{21}), which indicates that with proper gate bias adjustment there is no degradation to device performance due to TID. Additional tests should be performed to confirm that this result is reproducible.

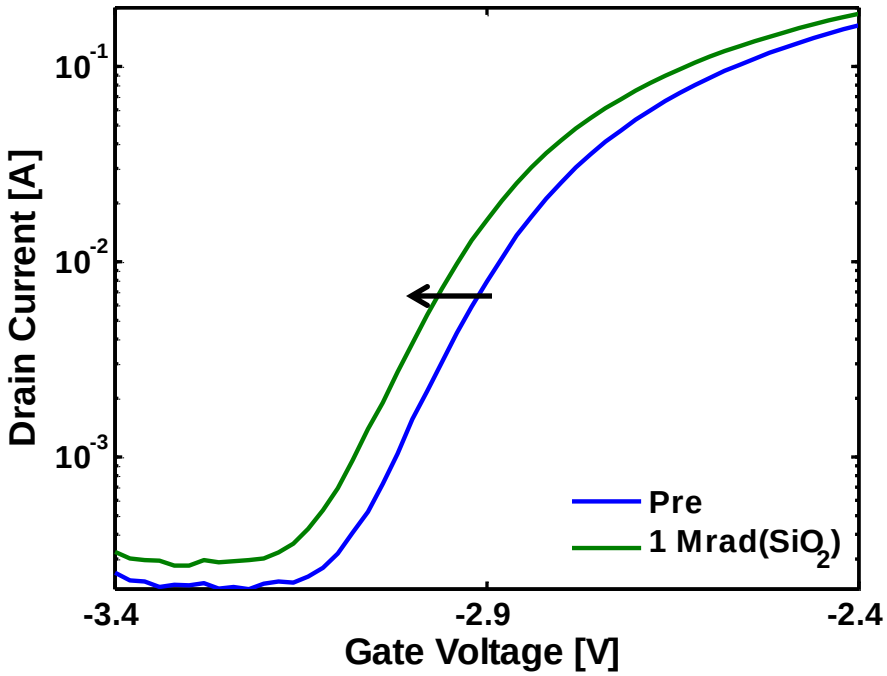

Fig. 5.1. Plot of I_D vs. V_G (V_D = 28 V) for the CGH40006P pre- and post-irradiation to 1 Mrad (SiO2) using 10 keV X-rays. Note the negative shift in threshold voltage.

Proton Test Results – DC Characteristics

Observing the DC characteristics allows insight into degradation mechanisms at the device level, and is essential for identifying potential failure modes. The DC current-voltage relationships were measured over various proton fluence levels using two devices from each manufacturer, for a total of four devices tested with protons. The plots of drain current (I_D) versus gate voltage (V_G) allow us to easily observe shifts in threshold voltage V_T. The transconductance g_m is defined by:

$$g_m = \frac{dI_D}{dV_G}$$

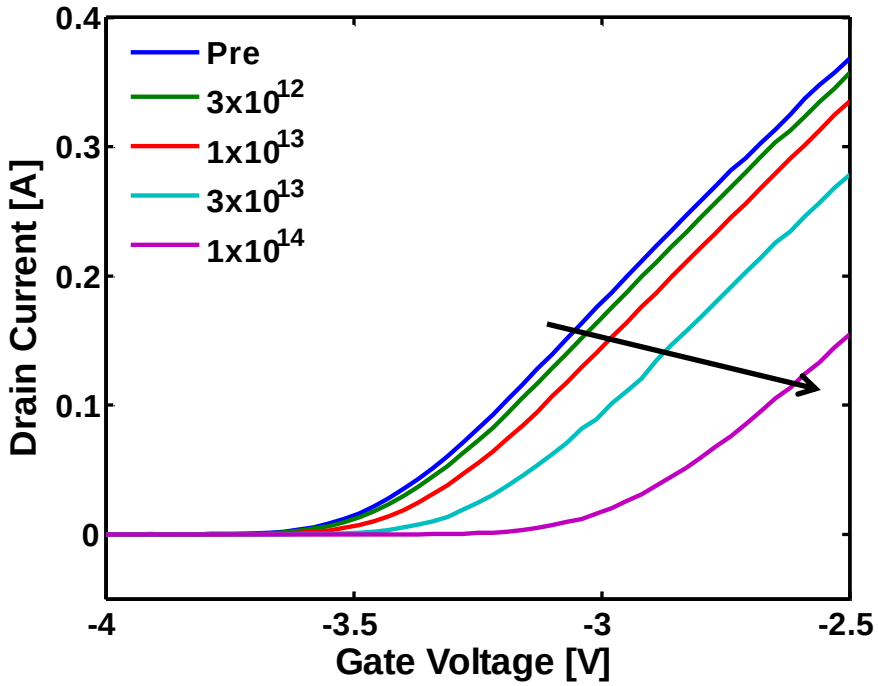

Fig. 5.2. Plot of I_D vs. V_G (V_D = 28 V) for the RF3826 as a function of proton fluence using 1.8 MeV protons up to total fluence of 10^{14} cm^{-2}. Note the monotonic positive increase in threshold voltage and decrease in slope with proton fluence.

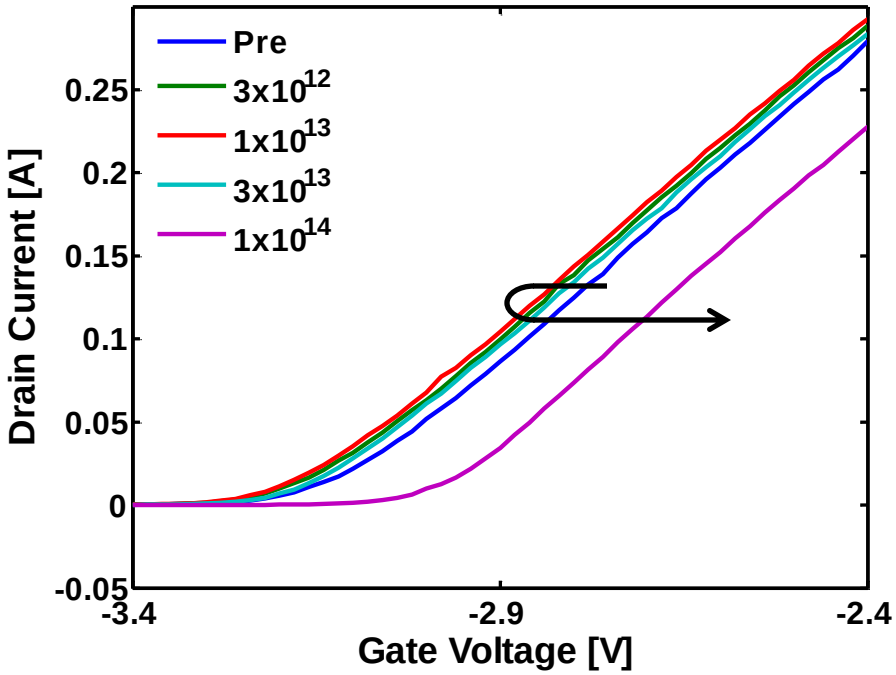

Fig. 5.3. Plot of I_D vs. V_G (V_D = 28 V) for the CGH40006P as a function of proton fluence using 1.8 MeV protons up to total fluence of 10^{14} protons/cm^2. Note the negative shift in V_T to a fluence of 10^{13} followed by a positive shift in V_T to a fluence of 10^{14} cm^{-2}.

Fig. 5.2 shows a positive shift in threshold voltage for the RFMD GaN HEMT that increases monotonically with proton fluence. Fig. 5.3 shows a different trend for the Cree GaN HEMT, starting with a negative shift in threshold voltage up to a fluence of 10^{13} cm^{-2}, and then it begins to shift in the positive direction up to a fluence of 10^{14} cm^{-2}. The largest total V_T shift for the CGH40006P was +0.22 V at the highest proton fluence. The largest total V_T shift of the RF3826 devices tested was +0.45 V at the highest proton fluence.

Fig. 5.4 shows g_m vs. V_G of the RF3826, in which it is evident that the peak transconductance decreases by 13-15% at a fluence of 10^{14} cm^{-2}. Fig. 5.5 shows g_m vs. V_G for the CGH40006P, which shows very little change to the peak transconductance even at the highest proton fluence level.

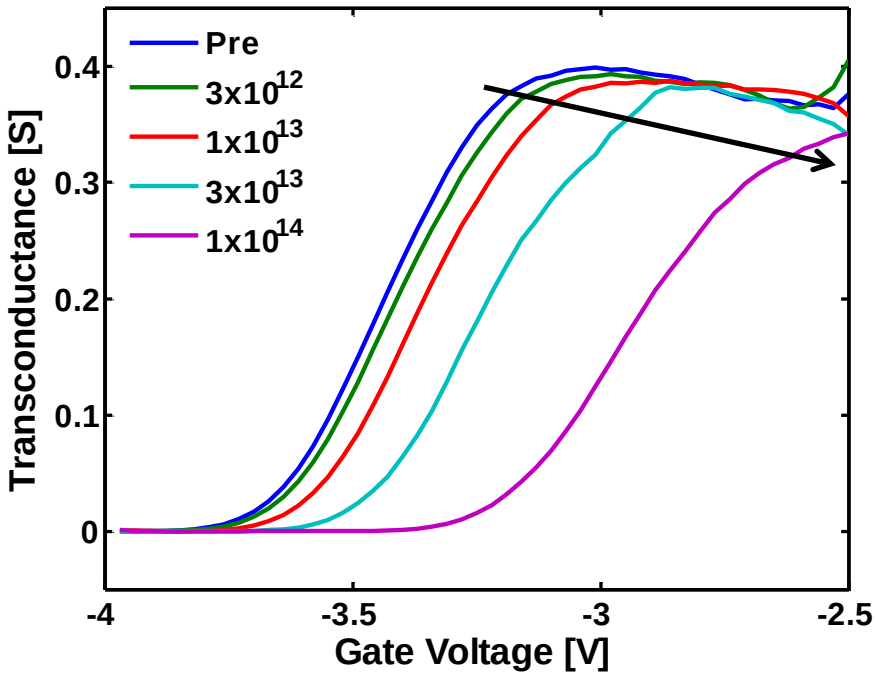

Fig. 5.4. Plot of g_m vs. V_G (V_D = 28 V) for the RF3826 as a function of proton fluence using 1.8 MeV protons up to a fluence of 10^{14} cm^{-2}. Note a decrease of ~15% in peak transconductance from pre-rad to 10^{14} cm^{-2}.

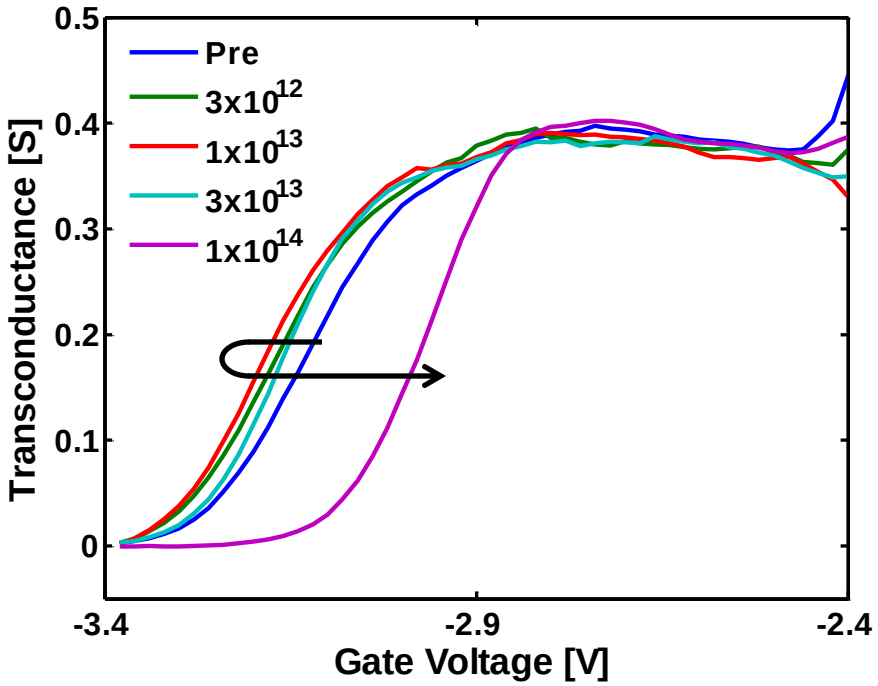

Fig. 5.5. Plot of g_m vs. V_G (V_D = 28 V) for the CGH40006P as a function of proton fluence using 1.8 MeV protons up to a fluence of 10^{14} cm^{-2}. Note that there is no significant change in the peak transconductance with proton fluence.

Two devices from each manufacturer were tested for proton-induced displacement damage using 1.8 MeV protons. For comparison purposes, a plot of threshold voltage vs. fluence for both manufacturers is provided in Fig. 5.6. This plot shows clearly the monotonic positive increase in threshold voltage for the RFMD devices. It also shows the initial negative threshold voltage shift and subsequent positive shift with proton fluence for the Cree devices.

The peak transconductance versus proton fluence is plotted in Fig. 5.7 for the two different devices. The RFMD devices show a decrease in transconductance, whereas the Cree devices show very little change in transconductance, and in fact show a higher transconductance at a fluence of 10^{14} cm^{-2}. We do not fully understand this phenomenon, which seems unphysical. Further testing should be performed to confirm this trend.

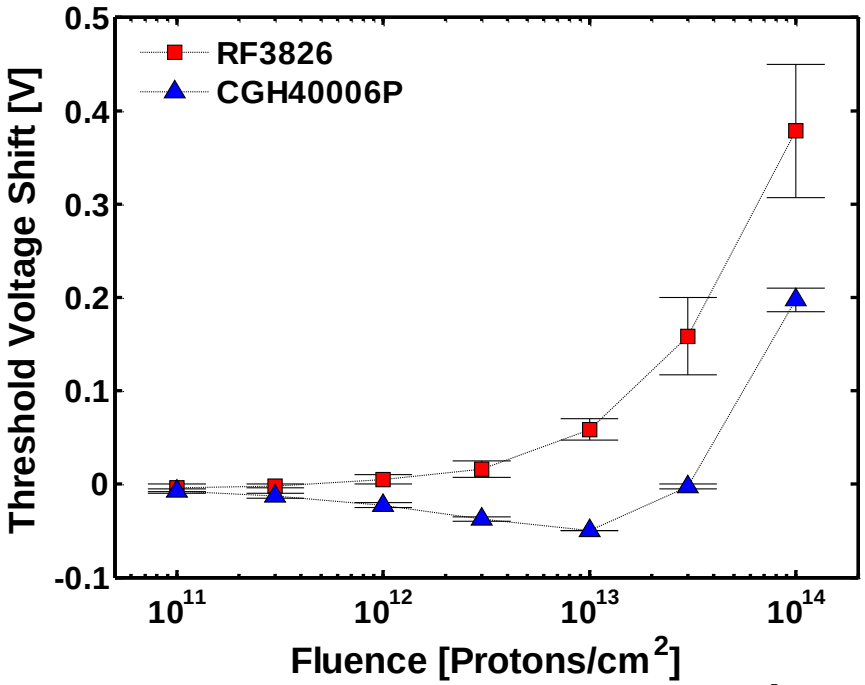

Fig. 5.6. Comparison of ΔV_T vs. proton fluence (cm^{-2}) for RFMD and Cree GaN HEMTs.

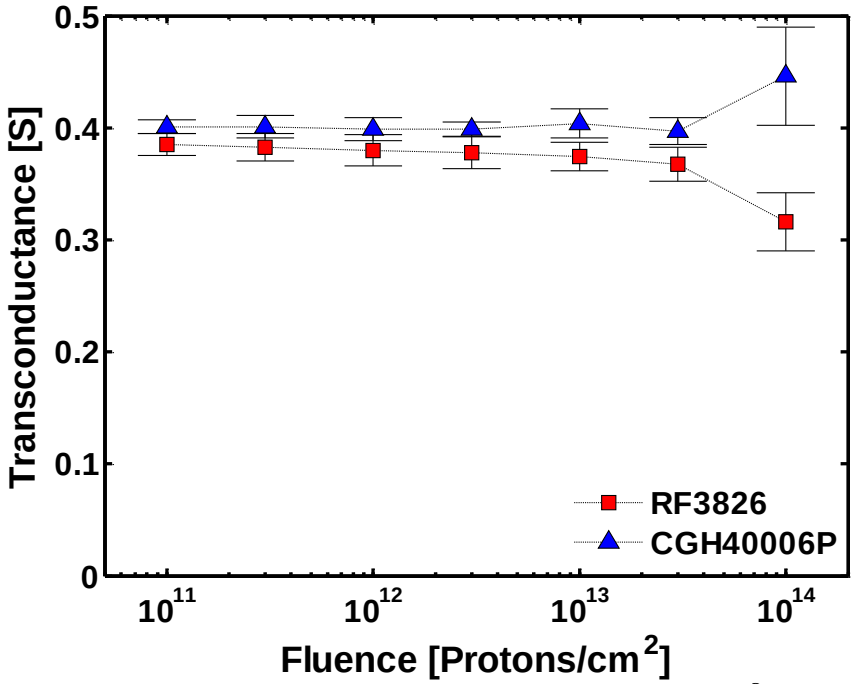

Fig. 5.7. Comparison of g_m vs. proton fluence (cm^{-2}) for RFMD and Cree GaN HEMTs.

Proton Test Results – S_{21} and Stability

In order to bias the GaN HEMT for RF amplification, both manufacturers suggest first applying a negative gate bias of -5 V and then applying a drain voltage of 28 V. The gate bias can then be increased until the drain current reaches the proper level. The recommended drain current for the RF3826 is 55 mA for a gain of 12 dB. The recommended drain current for the CGH40006P is 100 mA for a gain of 11-13 dB. Once the gate voltage was determined for each device that gives the recommended drain current (pre-irradiation), that gate voltage was used for all of the S-parameter measurements in order to demonstrate the effect of shifting threshold voltage on the RF characteristics of the amplifier.

Fig. 5.8 shows the forward gain (S_{21}) vs. frequency for the RF3826 as a function of proton fluence with fixed gate bias up to a fluence of 10^{14} cm^{-2}. After that point the gate voltage was adjusted to account for threshold voltage shift, which restored the drain current to its pre-irradiation value, and also restored the gain to near its pre-irradiation value. The same procedure was performed for the CGH40006P, as shown in figure 5.9. The black dotted lines in Figs. 5.8 and 5.9 represent S_{21} post-irradiation after the gate voltage has been adjusted.

The post-irradiation S_{21} for the RF3826 was only reduced by a small amount even at the highest fluence. By converting the gain from dB to power ratio, it was determined that S_{21} was reduced by about 15%, which corresponds to a similar reduction in g_m seen in the same device. Interestingly, the forward gain of the CGH40006P is nearly the same pre- and post-irradiation when the gate voltage is adjusted, which corresponds well with the negligible change in peak g_m seen in the same device.

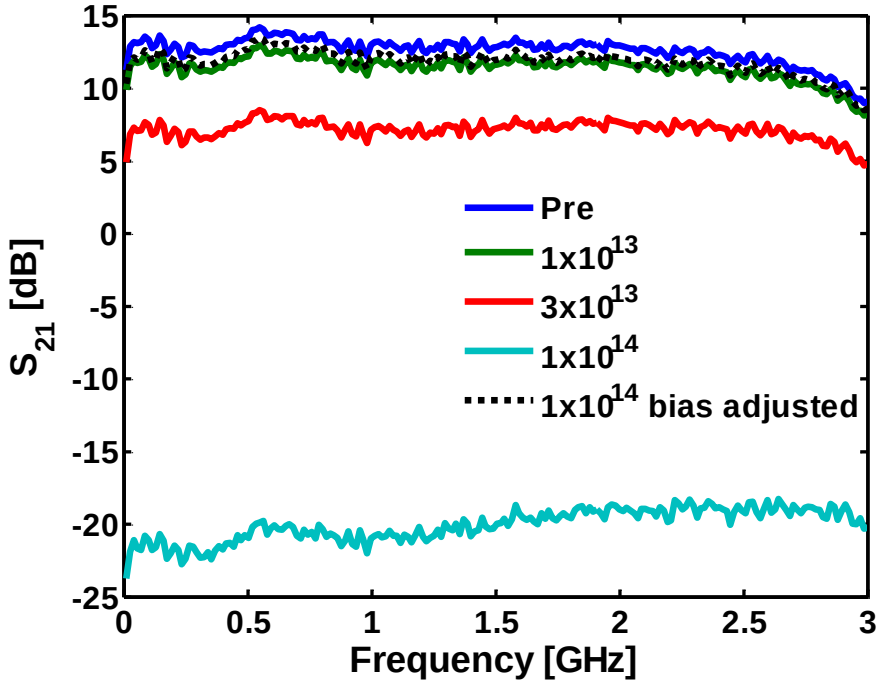

Fig. 5.8. Forward gain (S_{21}) vs. frequency as a function of proton fluence (cm^{-2}) for the RF3826. Fixed bias was used for all measurements up to a fluence of 10^{14} cm^{-2}. Post-irradiation, the bias was adjusted to account for threshold voltage shift and restore gain.

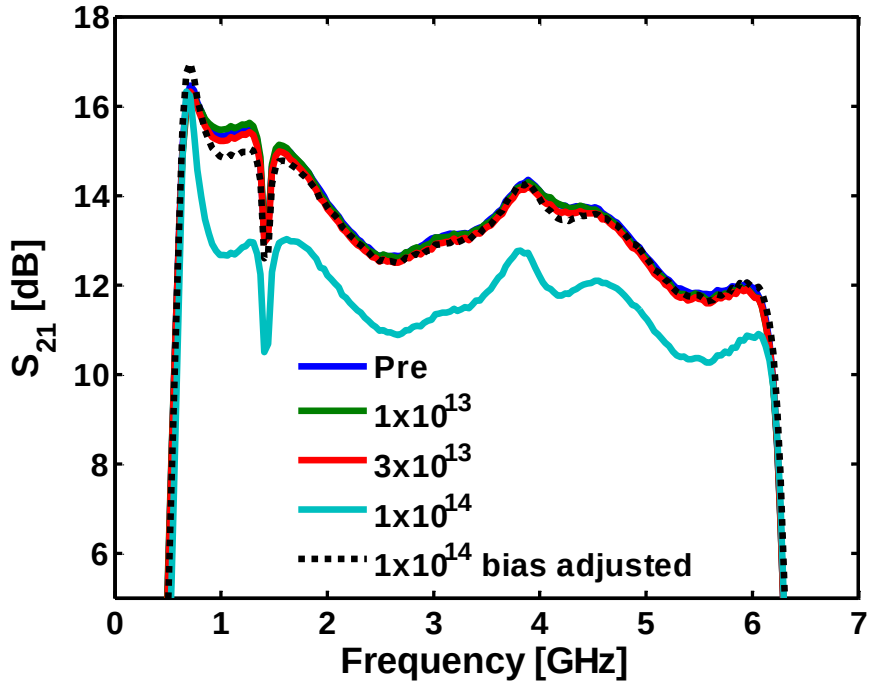

Fig. 5.9. Forward gain (S_{21}) vs. frequency as a function of proton fluence (cm^{-2}) for the CGH40006P. The same procedures were used as in Fig. 5.8.

The Rollett stability factors K and Δ were evaluated using the S-parameters of both devices. The values K > 1 and Δ < 1 indicate unconditional stability at a particular frequency. Both sets of devices are unconditionally stable pre- and post-irradiation over their intended bandwidth with proper DC bias, as shown in Figs. 5.10 and 5.11. The RF3826 only shows regions of instability (K < 1) post-irradiation if the gate bias is fixed and the threshold voltage shift causes the drain current to drastically fall off (not shown). But under this condition, the gain is much below unity (-20 dB) so oscillation is not a primary concern. Similarly, the CGH40006P shows a region of instability (K < 1) pre-irradiation at 0.3 GHz at nominal bias. However, the gain S_{21} is below unity at 0.3 GHz, making oscillatory behavior irrelevant. Unwanted oscillatory behavior does not occur for either type of GaN HEMT when gain is above unity.

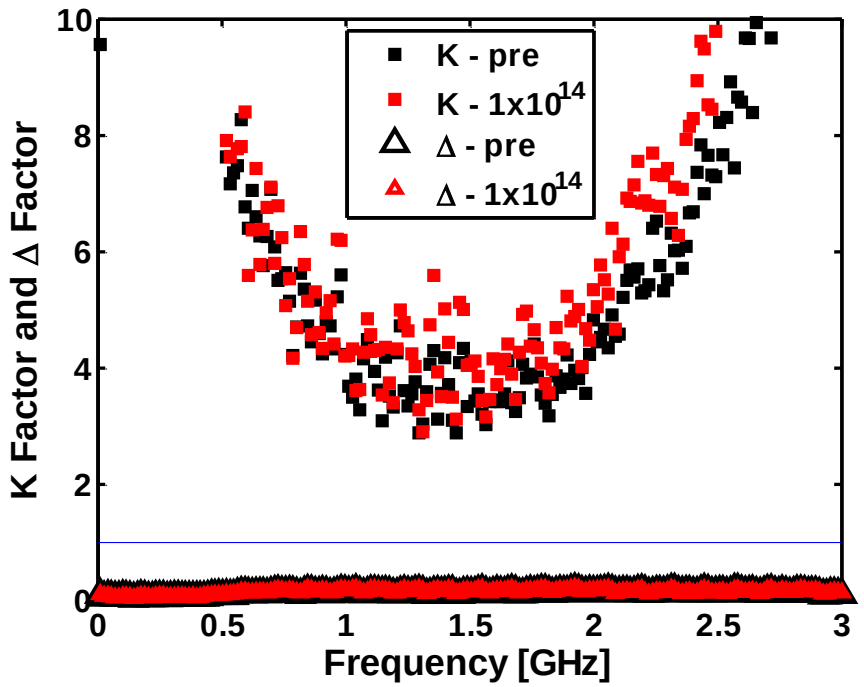

Fig. 5.10. Rollett stability factors K and Δ vs. frequency pre- and post-irradiation for the RF3826. The post-irradiation Rollett stability factors are at a fluence of 10^{14} cm^{-2} after the gate bias has been adjusted to account for threshold voltage shift. Note that K and Δ indicate unconditional stability across the entire bandwidth. A blue reference line indicates K = 1 or Δ = 1.

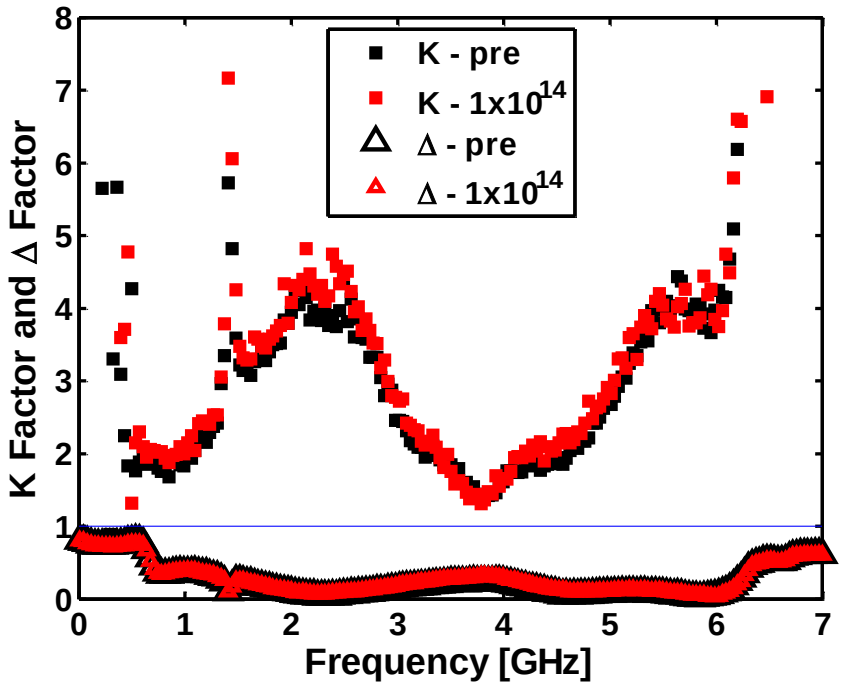

Fig. 5.11. Rollett stability factors K and Δ vs. frequency pre- and post-irradiation for the CGH40006P. The post-irradiation Rollett stability factors are at a fluence of 10^{14} cm^{-2} after the gate bias has been adjusted to account for threshold voltage shift. Note that a value of K < 1 exists at 0.3 GHz, although it is not clearly evident in this plot.

The fact that the stability factor is unaffected after high levels of proton-induced displacement damage is a surprising result. Any changes to the input and output impedance of the GaN HEMT caused by displacement damage do not appear to affect the impedance matching of the RF amplifier circuit. This was a concern, especially since a previous study attributed degradation of RF parameters to impedance mismatch [22].

Proton Test – RF Gain

The small signal S-parameters are very important for determining the small signal gain and reflection coefficients of an amplifier, and allow us to analyze the Rollett stability factor. However, since they use small signals on the order of -10 dBm, they don't give us insight into the impacts of displacement damage on RF output power and power efficiency. Figs. 5.12 and 5.13 show RF gain vs. P_{in} as a function of proton fluence.

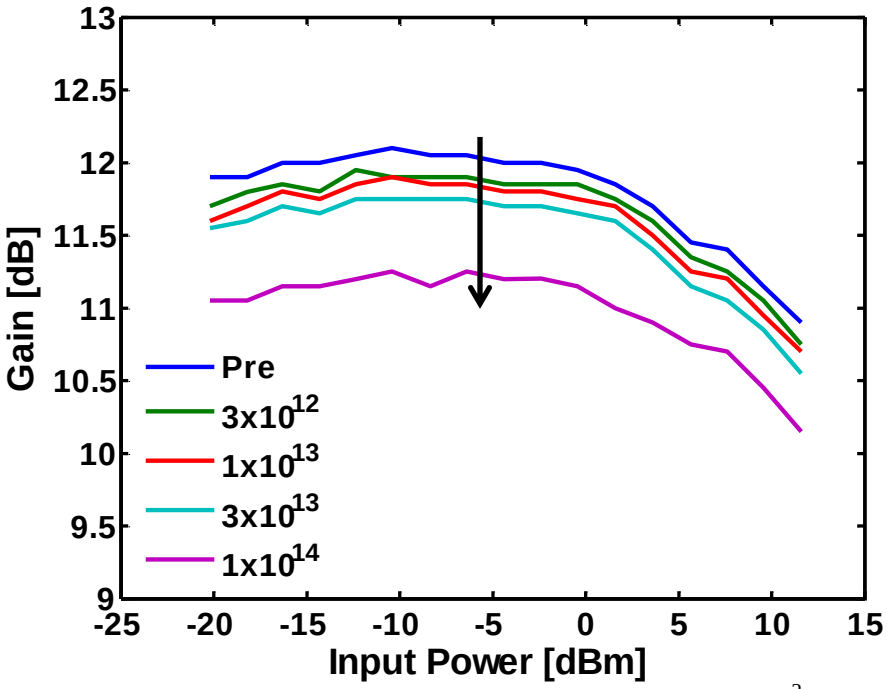

Fig. 5.12. Gain vs. input power as a function of proton fluence (cm^{-2}) for the RF3826. Gate voltage was adjusted after each irradiation step to account for threshold voltage shift and maintain a constant drain current during each measurement. (f = 1 GHz).

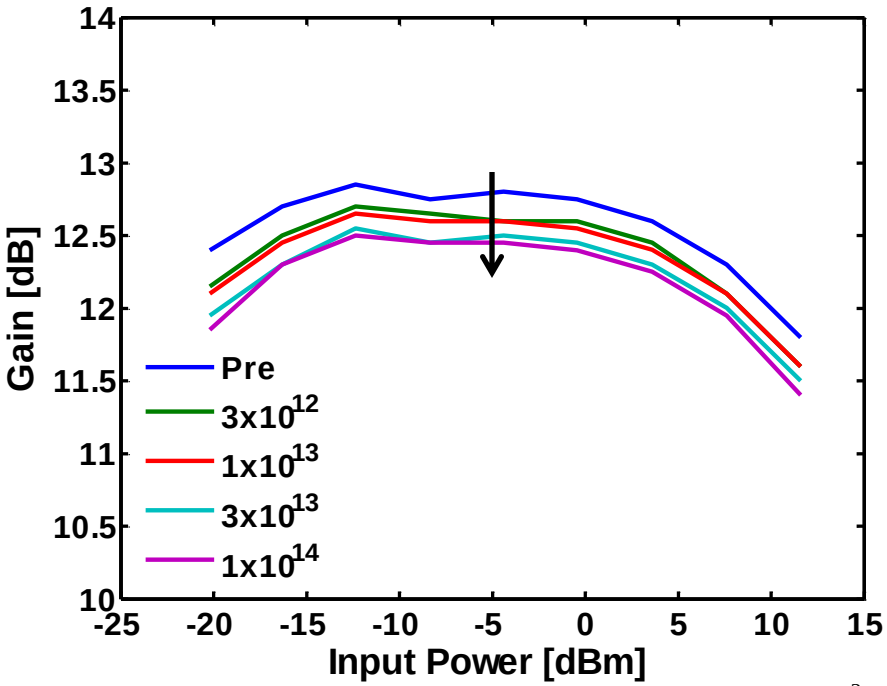

Fig. 5.13. Gain vs. input power as a function of proton fluence (cm^{-2}) for the CGH40006P. The same procedures were used as in Fig. 5.12. (f = 2 GHz).

The RF gain in Figs. 5.12 and 5.13 shows a trend of decreased RF output power with proton fluence. The highest-fluence decrease in RF gain for the RF3826 was 0.8 dB or about 16% of the total gain in Watts per Watt. The decrease in RF gain for the CGH40006P was 0.35 dB or about 7% of the total gain in Watts per Watt.

The Cree GaN HEMTs show less decrease in S_{21} and RF gain than the RFMD GaN HEMTs due to proton irradiation. This result is interesting since the Cree GaN HEMTs show a small shift in threshold voltage due to X-ray irradiation, while the RFMD devices show no TID effects. It may be the case that the competing physical mechanisms that cause negative and positive threshold voltage shifts in the Cree devices help to mitigate the effects at large proton fluences.

A very important figure of merit for RF transistor amplifiers is power efficiency. Some manufacturers list the drain efficiency (η_{drain}), while other manufacturers list the

power-added efficiency (PAE) of their GaN HEMTs. Power efficiency is generally defined using the following equations:

$$\eta_{drain} = \frac{P_{RFout}}{P_{DC}} = \frac{P_{RFout}}{I_{DC} \times V_{DC}}$$

$$PAE = \frac{(P_{RFout} - P_{RFin})}{P_{DC}} = \frac{(P_{RFout} - P_{RFin})}{I_{DC} \times V_{DC}}$$

Clearly, as the output power decreases with proton fluence for a given input power, the drain efficiency and PAE will also decrease. This is a major concern for the designer who must design an amplifier with a particular efficiency. If displacement damage decreases the efficiency of the amplifier, it may be possible to achieve the proper gain by increasing the drain bias current. But the side effect of higher drain current will be higher dissipated power and heat in the amplifier. Dissipated heat may create additional problems with efficiency. GaN HEMTs are notorious for self-heating effects that may decrease device performance over time [9].

CHAPTER VI

Conclusions

The experimental results from Chapter V give insight into the radiation hardness of commercial GaN HEMTs intended for RF power amplifier applications. GaN HEMTs from RFMD show no susceptibility to TID effects up to a dose of 1 Mrad (SiO_2) using 10 keV X-rays. Given that the RFMD GaN HEMTs do not show any effects at this dose, it is unlikely that TID will contribute as much damage as lattice displacement [12]. However, the Cree GaN HEMT that was irradiated with X-rays showed a small shift in V_T at 1 Mrad (SiO_2). Both types of devices were exposed to a relatively high proton fluence of 10^{14} p+ cm^{-2}, which corresponds to a total ionizing dose of about 110 Mrad (GaN) using Table 4 to convert from fluence to Mrad. This is quite a large amount of protons, and could possibly take decades in satellite orbit to accumulate this much damage. However, a solar disturbance such as a coronal mass ejection could contribute a similar amount of proton fluence in only a few minutes or hours [11].

The 2-port S-parameters, Rollett stability factors, and RF gain only show minimal, changes due to X-rays or protons as long as the devices maintain a constant drain bias current by adjusting the gate voltage. A feedback mechanism that monitors the drain current and adjusts the gate bias would be necessary to ensure that the gain does not decrease by more than 16% at a fluence of 10^{14} cm^{-2}. External bias circuitry with feedback should be used for these devices in radiation environments, rather than fixing the gate bias using laser trimming or fuse trimming techniques.

At the highest proton fluence tested for these devices, both amplifiers still appear to function well and provide about 12 dB of gain. However, since the output power and gain are decreased slightly for a given input power, this will affect the power-added efficiency (PAE) of the amplifier circuit. More power will be dissipated in order to maintain these devices in the intended mode of operation with sufficient gain. Increased temperature may cause further decrease in amplifier performance due to the self-heating effects of GaN HEMTs.

The negative effects of displacement damage can be improved by a process of thermal annealing at room temperature or at elevated temperatures. Sometimes several weeks at room temperature are enough to remove defects [17], [20]. Cai et al. showed that a rapid thermal anneal (RTA) at 800° C removes most of the defects and drastically improved the device performance post-irradiation [33]. It is reasonable to conclude that GaN HEMTs used in RF power applications would be at elevated temperatures during operation, and would mitigate many of the effects of displacement damage. More damage would accumulate when the circuit is powered off than during operation. Temporarily increasing the drain current or increasing the temperature by other means would likely ensure the GaN HEMTs show little or no degradation even in proton abundant environments.

The commercial GaN HEMTs studied in this work appear to be very robust to both ionizing and non-ionizing radiation over time as long as gate bias is adjusted for V_T shift, and offer superior performance in proton-rich radiation environments. Single event effects may prove to be a much greater concern for these types of devices, and further studies should focus on degradation and failure modes caused by heavy ions.

REFERENCES

[1] U. K. Mishra and T. E. Kazior, "GaN-based RF power devices and amplifiers," *Proc. IEEE*, vol. 96, no. 2, pp. 287–305, Feb. 2008.

[2] Y.-F. Wu, D. Kapolnek, J. P. Ibbetson, P. Parikh, B. P. Keller, and U. K. Mishra, "Very-high power density AlGaN/GaN HEMTs," *IEEE Trans. Electron Devices*, vol. 48, no. 3, pp. 586–590, Mar. 2001.

[3] G. Meneghesso, G. Verzellesi, F. Danesin, F. Rampazzo, F. Zanon, A. Tazzoli, M. Meneghini, and E. Zanoni, "Reliability of GaN high-electron-mobility transistors : state of the art and perspectives," *IEEE Trans. Device Mater. Reliab.*, vol. 8, no. 2, pp. 332–343, 2008.

[4] S. M. Sze and M. K. Lee, *Semiconductor Devices Physics and Technology*, 3rd Editio. New York: Wiley, 2012, pp. 249–255.

[5] P. M. Solomon and H. Morkoc, "Modulation-doped GaAs/AlGaAs heterojunction field-effect transistors (MODFET's), ultrahigh-speed device for supercomputers," *IEEE Trans. Electron Devices*, vol. 31, no. 8, pp. 1015–1027, 1984.

[6] L. Esaki and R. Tsu, "Superlattice and negative differential conductivity in semiconductors," *IBM J. Res. Dev.*, vol. 14, no. 1, pp. 61–65, 1970.

[7] R. Dingle, H. L. Störmer, A. C. Gossard, and W. Wiegmann, "Electron mobilities in modulation-doped semiconductor heterojunction superlattices," *Appl. Phys. Lett.*, vol. 33, no. 7, p. 665, 1978.

[8] M. Asif Khan, a. Bhattarai, J. N. Kuznia, and D. T. Olson, "High electron mobility transistor based on a GaN-AlxGa1−xN heterojunction," *Appl. Phys. Lett.*, vol. 63, no. 9, p. 1214, 1993.

[9] S. A. Vitusevich, A. M. Kurakin, N. Klein, M. V. Petrychuk, A. V. Naumov, and A. E. Belyaev, "AlGaN/GaN high electron mobility transistor structures: self-heating effect and performance degradation," *IEEE Trans. Device Mater. Reliab.*, vol. 8, no. 3, pp. 543–548, Sep. 2008.

[10] Y. S. Puzyrev, T. Roy, E. X. Zhang, D. M. Fleetwood, R. D. Schrimpf, and S. T. Pantelides, "Radiation-induced defect evolution and electrical degradation of AlGaN/GaN high-electron-mobility transistors," *IEEE Trans. Nucl. Sci.*, vol. 58, no. 6, pp. 2918–2924, 2011.

[11] D. M. Fleetwood and P. S. Winokur, "Radiation effects in the space telecommunications environment," *PROC. 22nd Int. Conf. Microelectron. (MIEL 2000)*, vol. 1, pp. 43–49, 2000.

[12] B. Luo, J. W. Johnson, F. Ren, K. K. Allums, C. R. Abernathy, S. J. Pearton, A. M. Dabiran, A. M. Wowchack, C. J. Polley, P. P. Chow, D. Schoenfeld, and A. G. Baca, "Influence of 60Co γ-rays on dc performance of AlGaN/GaN high electron mobility transistors," *Appl. Phys. Lett.*, vol. 80, no. 4, pp. 604–606, 2002.

[13] O. Aktas, a. Kuliev, V. Kumar, R. Schwindt, S. Toshkov, D. Costescu, J. Stubbins, and I. Adesida, "60Co gamma radiation effects on DC, RF, and pulsed I–V characteristics of AlGaN/GaN HEMTs," *Solid. State. Electron.*, vol. 48, no. 3, pp. 471–475, Mar. 2004.

[14] L. Scheick, "Determination of single-event effect application requirements for enhancement mode gallium nitride HEMTs for use in power distribution circuits," *IEEE Trans. Nucl. Sci.*, vol. 61, no. 6, pp. 2881–2888, Dec. 2014.

[15] X. Sun, O. I. Saadat, J. Chen, E. X. Zhang, S. Cui, T. Palacios, D. M. Fleetwood, and T. P. Ma, "Total-ionizing-dose radiation effects in AlGaN/GaN," *IEEE Trans. Nucl. Sci.*, vol. 60, no. 6, pp. 4074–4079, 2013.

[16] X. Hu, A. P. Karmarkar, B. Jun, D. M. Fleetwood, R. D. Schrimpf, R. D. Geil, R. A. Weller, B. D. White, M. Bataiev, L. J. Brillson, and U. K. Mishra, "Proton-Irradiation Effects on AlGaN/AlN/GaN High Electron Mobility Transistors," *IEEE Trans. Nucl. Sci.*, vol. 50, no. 6, pp. 1791–1796, 2003.

[17] X. Hu, B. K. Choi, H. J. Barnaby, D. M. Fleetwood, R. D. Schrimpf, S. Lee, S. Shojah-Ardalan, R. Wilkins, U. K. Mishra, and R. W. Dettmer, "The energy dependence of proton-induced degradation in AlGaN/GaN high electron mobility transistors," *IEEE Trans. Nucl. Sci.*, vol. 51, no. 2, pp. 293–297, Apr. 2004.

[18] A. Kalavagunta, A. Touboul, L. Shen, R. D. Schrimpf, R. A. Reed, D. M. Fleetwood, R. K. Jain, and U. K. Mishra, "Electrostatic mechanisms responsible for device degradation in proton irradiated AlGaN/AlN/GaN HEMTs," *IEEE Trans. Nucl. Sci.*, vol. 55, no. 4, pp. 2106–2112, Aug. 2008.

[19] A. Johnston, *Reliability and Radiation Effects in Compound Semiconductors*. Singapore: World Scientific, 2010, p. 241.

[20] J. W. McClory and J. C. Petrosky, "Temperature dependent electrical characteristics of neutron irradiated AlGaN/GaN HFETs," *IEEE Trans. Nucl. Sci.*, vol. 54, no. 6, pp. 1969–1974, 2007.

[21] A. Kalavagunta, M. Silvestri, M. J. Beck, S. K. Dixit, R. D. Schrimpf, R. A. Reed, D. M. Fleetwood, L. Shen, and U. K. Mishra, "Impact of proton irradiation-induced bulk defects on gate-lag in GaN HEMTs," *IEEE Trans. Nucl. Sci.*, vol. 56, no. 6, pp. 3192–3195, 2009.

[22] J. Chen, E. X. Zhang, C. X. Zhang, M. W. Mccurdy, D. M. Fleetwood, R. D. Schrimpf, S. W. Kaun, E. C. H. Kyle, and J. S. Speck, "RF performance of proton-irradiated AlGaN/GaN HEMTs," *IEEE Trans. Nucl. Sci.*, vol. 61, no. 6, pp. 2959–2964, 2014.

[23] G. Sonia, F. Brunner, A. Denker, R. Lossy, M. Mai, J. Opitz-Coutureau, G. Pensl, E. Richter, J. Schmidt, U. Zeimer, L. Wang, M. Weyers, J. Würfl, and G. Tränkle, "Proton and heavy ion irradiation effects on AlGaN / GaN HFET devices," *IEEE Trans. Nucl. Sci.*, vol. 53, no. 6, pp. 3661–3666, 2006.

[24] I. K. Samsel, E. X. Zhang, N. C. Hooten, E. D. Funkhouser, W. G. Bennett, R. A. Reed, R. D. Schrimpf, M. W. Mccurdy, D. M. Fleetwood, R. A. Weller, G. Vizkelethy, X. Sun, T.-P. Ma, O. I. Saadat, and T. Palacios, "Charge collection mechanisms in AlGaN/GaN MOS high electron mobility transistors," *IEEE Trans. Nucl. Sci.*, vol. 60, no. 6, pp. 4439–4445, 2013.

[25] S. Liu, M. Boden, D. A. Girdhar, and J. L. Titus, "Single-event burnout and avalanche characteristics of power DMOSFETs," *IEEE Trans. Nucl. Sci.*, vol. 53, no. 6, pp. 3379–3385, 2006.

[26] S. Bazzoli, S. Girard, J. Baggio, P. Paillet, and O. Duhamel, "SEE sensitivity of a COTS GaN transistor and silicon MOSFETs," *Radiat. Its Eff. Components Syst. 2007. RADECS 2007. 9th Eur. Conf.*, pp. 1–5, 2007.

[27] S. Kuboyama, A. Maru, H. Shindou, N. Ikeda, T. Hirao, H. Abe, and T. Tamura, "Single-event damages caused by heavy ions observed in AlGaN / GaN HEMTs," *IEEE Trans. Nucl. Sci.*, vol. 58, no. 6, pp. 2734–2738, 2011.

[28] M. Rostewitz, K. Hirche, J. Lätti, and E. Jutzi, "Single event effect analysis on DC and RF operated AlGaN/GaN HEMTs," *IEEE Trans. Nucl. Sci.*, vol. 60, no. 4, pp. 2525–2529, 2013.

[29] G. Gonzalez, *Microwave Transistor Amplifiers Analysis and Design*. Englewood Cliffs, N.J.: Prentice-Hall, 1984, pp. 95–99.

[30] J. Rollett, "Stability and power-gain invariants of linear twoports," *IRE Trans. Circuit Theory*, vol. 9, no. 1, pp. 1–4, 1962.

[31] R. P. Meys, "Review and discussion of stability criteria for linear 2-ports," *IEEE Trans. Circuits Syst.*, vol. 37, no. 11, pp. 1450–1452, 1990.

[32] M. L. Edwards and J. H. Sinsky, "A new criterion for linear 2-port stability using a single geometrically derived parameter," *IEEE Trans. Microw. Theory Tech.*, vol. 40, no. 12, pp. 2303–2311, 1992.

[33] S. J. Cai, Y. S. Tang, R. Li, Y. Y. Wei, L. Wong, Y. L. Chen, K. L. Wang, M. Chen, Y. F. Zhao, R. D. Schrimpf, J. C. Keay, and K. F. Galloway, “Annealing behavior of a proton irradiated AlxGa1-xN/GaN high electron mobility transistor grown by MBE,” *IEEE Trans. Electron Devices*, vol. 47, no. 2, pp. 304–307, 2000.